Electron-Transfer Induced Repair of 6-4 Photoproducts in DNA: A Computational Study

O. Anders Borg,[†] Leif A. Eriksson,[‡] and Bo Durbeej*[,§]

Department of Quantum Chemistry, Uppsala University, Box 518, S-751 20, Uppsala, Sweden, Department of Natural Sciences and Örebro Life Science Center, Örebro University, Fakultetsgatan 1, S-701 82, Örebro, Sweden, and Department of Chemistry, University of Siena, Via Aldo Moro 2, I-53100, Siena, Italy

Received: November 16, 2006; In Final Form: January 18, 2007

The mechanism employed by DNA photolyase to repair 6-4 photoproducts in UV-damaged DNA is explored by means of quantum chemical calculations. Considering the repair of both oxetane and azetidine lesions, it is demonstrated that reduction as well as oxidation enables a reversion reaction by creating anionic or cationic radicals that readily fragment into monomeric pyrimidines. However, on the basis of calculated reaction energies indicating that electron transfer from the enzyme to the lesion is a much more favorable process than electron transfer in the opposite direction, it is suggested that the photoenzymic repair can only occur by way of an anionic mechanism. Furthermore, it is shown that reduction of the oxetane facilitates a mechanism involving cleavage of the C−O bond followed by cleavage of the C−C bond, whereas reductive fragmentation of the azetidine may proceed with either of the intermonomeric C−N and C−C bonds cleaved as the first step. From calculations on neutral azetidine radicals, a significant increase in the free-energy barrier for the initial fragmentation step upon protonation of the carbonylic oxygens is predicted. This effect can be attributed to protonation serving to stabilize reactant complexes more than transition structures.

Introduction

UV radiation is known to cause structural alterations of nucleic acids, which may sterically inhibit the enzymes responsible for DNA transcription and replication and thereby induce apoptosis or the development of skin cancer.[1−4] The most common UV-induced DNA damages are the cyclobutane pyrimidine dimers (CPD) and the pyrimidine (6-4) pyrimidone photoproducts (6-4 photoproducts).[5,6] These are formed from two adjacent pyrimidine (Pyr) nucleobases of the same DNA strand upon exposure to far-UV radiation (200−300 nm).[5,6] The formation and repair of CPDs, which constitute 80−90% of the lesions observed,[5] have been studied extensively by means of both experimental techniques and theoretical computations.[5−19]

Perhaps the most ingenious enzymatic repair system for the protection against accumulation of CPD lesions is provided by electron-transferring DNA photolyases.[5−7,9,10] The activity of these enzymes is governed by a light-harvesting cofactor (either methenyltetrahydrofolate (MTHF) or 8-hydroxy-5-deazariboflavin (8-HDF)) and a catalytic cofactor (always the deprotonated $FADH^-$ form of 1,5-dihydroflavin adenine dinucleotide ($FADH_2$)). The photoenzymic repair process is initiated by absorption of near-UV and visible light (300−500 nm) by the light-harvesting cofactor, followed by excitation-energy transfer to the catalytic cofactor. The subsequent steps serving to destabilize the lesion have remained a subject of much controversy for a long time, with mechanisms involving electron transfer (ET) either from the catalytic cofactor to the CPD lesion or from the CPD lesion to the catalytic cofactor being advocated.[10,20,21] Today, it has been established that the photoenzymic repair is accomplished through the formation of a CPD radical anion, which readily fragments into a closed-shell monomeric Pyr (i.e., the parent thymine (T) or cytosine (C)) and an open-shell monomeric Pyr radical anion (i.e., the parent T or C in its reduced form).[5,6] Finally, the excess electron of the reduced Pyr is transferred back to the catalytic cofactor, which restores the resting state of the enzyme.

The 6-4 photoproducts, in turn, make up 10−20% of the UV-induced DNA lesions.[5] The formation of these has been shown to proceed via cyclic oxetane/azetidine intermediates resulting from the cycloaddition of the C5═C6 and C4′═O/NH bonds of two excited Pyrs (Figure 1).[5,6] This type of [2 + 2] cycloaddition is commonly known as the Paterno−Büchi reaction.[22] The thermodynamically more stable[23] 6-4 photoproducts are then formed through proton or hydrogen-atom transfer from N3′ to the O/N heteroatom of the oxetane/azetidine, which is linked to the breakage of the C4′−O/NH bond.[6,7] The cyclic intermediates (T+T oxetane, C+T oxetane, T+C azetidine, and C+C azetidine) leading to the four possible 6-4 photoproducts are shown in Figure 1.

It has been demonstrated that 6-4 photoproducts are efficiently repaired by catalytic nucleotide- and base-excision repair systems.[5,24] In addition, from 1993 onward, DNA photolyases exclusively recognizing and repairing 6-4 photoproducts have been discovered in many organisms.[25−29] The mechanistic action of these enzymes, which are not as well-characterized as the CPD photolyases, is still the subject of much research.[27,30,31] Since the O/N heteroatom is transferred from one Pyr moiety to the other during photoproduct formation, photoenzymic repair accomplished by direct splitting of the lesion would not recover the parent Pyrs but would yield structurally modified nucleobases. Such structures are, however, not observed experimentally. Accordingly, it has been proposed that the repair proceeds via the initial regeneration of the oxetane/azetidine.[27,32] Such a

* Corresponding author. E-mail: bo.durbeej@kvac.uu.se.
[†] Uppsala University.
[‡] Örebro University.
[§] University of Siena.

10.1021/jp0676383 CCC: $37.00
Published on Web 03/07/2007

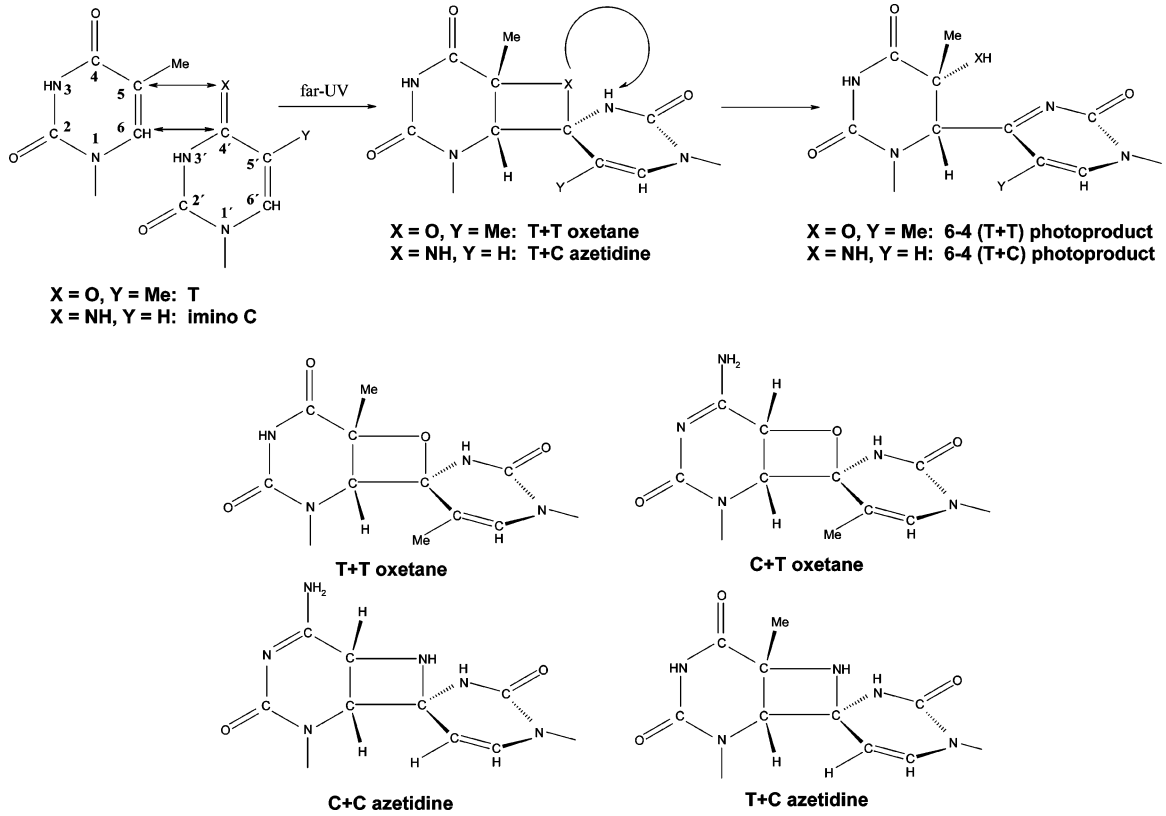

Figure 1. (Top) Formation of 6-4 photoproducts in UV-irradiated DNA. (Bottom) Different cyclic oxetane and azetidine intermediates in the UV-induced formation of 6-4 photoproducts in DNA.

mechanism would resemble that employed by CPD photolyases and is indirectly implicated by the similarity between CPD and 6-4 photolyases in terms of structure and binding of cofactors.[33]

A tentative mechanism for the photoenzymic repair of 6-4 photoproducts can be outlined as follows. First, the enzyme recognizes and binds to the damaged DNA and flips the lesion into a cavity of the enzyme.[26,34] Two histidines are then involved in regenerating the cyclic intermediate. One is responsible for making C4′ more prone to nucleophilic attack by adding a proton to N3′, and the other removes a proton from the C5 OH/NH2 group. Thereby, a nucleophilic attack of O^-/NH^- on C4′ is enabled, resulting in the formation of the oxetane/azetidine.[35] In analogy with the mechanism underlying the catalytic activity of CPD photolyases, the light-harvesting cofactor then absorbs light and the excitation energy is transferred to the catalytic cofactor.[5,26] Furthermore, mediated by ET of the excited catalytic cofactor either to or from the oxetane/azetidine, both anionic and cationic reaction mechanisms are conceivable also for the photoenzymic repair of this type of DNA lesion. However, in contrast to the consensus view on the mechanism of CPD photolyases,[5,6] *direct* experimental evidence for the ET of 6-4 photolyases occurring from the catalytic cofactor to the oxetane/azetidine is, to the best of our knowledge, yet to be reported.

A wide variety of model systems have been employed in experimental investigations of the mechanism of 6-4 photolyases.[36−39] Parallel to the numerous quantum chemical studies that have made important contributions to the understanding of how CPD photolyases function,[13−17] 6-4 lesions have also been the subject of theoretical computations.[23,40,41] To date, however, no extensive investigation of ET-induced repair of 6-4 photoproducts using state-of-the-art quantum chemical methods has been performed. Given the lack of high-level computational data, the aim of the present work is to explore anionic as well as cationic reaction mechanisms for the regeneration of the native Pyrs from both oxetane and azetidine lesions by means of density functional theory (DFT) calculations. Since both reduction[28,42] and oxidation[43,44] appear to facilitate cycloreversion, a comparison between the two mechanisms in terms of energetics is made in order to deduce whether either is more favorable from the point of view of its intrinsic (i.e., neglecting the influence of the surrounding enzyme) chemical features. For this purpose, the energetics obtained for a noncatalyzed (i.e., non-radical) cycloreversion reaction are used as reference data.

Methods

The study concerns the photoenzymic repair of one oxetane (T+T, Figure 1) and one azetidine (T+C, Figure 1). Apart from the two Pyrs directly involved in the formation of the lesion, the computational model systems also include the two deoxyriboses (2-deoxy-D-ribose) bound to the Pyrs and the phosphate group connecting these. It is assumed that the stereochemistry of the oxetane/azetidine H4′ atom (*Z* or *E* with respect to the four-membered ring) does not play an important role for the repair mechanism, and therefore only *Z* configurations are considered. In order for the overall charge of the computational models to equal the overall charge of the two Pyrs, the phosphate group is kept protonated.

Calculations were carried out for closed-shell (neutral) and open-shell (anionic and cationic) states of T+T oxetane and T+C azetidine. Two different fragmentation pathways were explored for open-shell species (Figure 2): (i) breakage of the C6−C4′ bond followed by breakage of the C5−X4′ bond, below referred to as CC−CX and proceeding either via transition structures TS1CCan and TS2CXan (anionic pathway, Figure 2) or via TS1CCcat and TS2CXcat (cationic pathway,

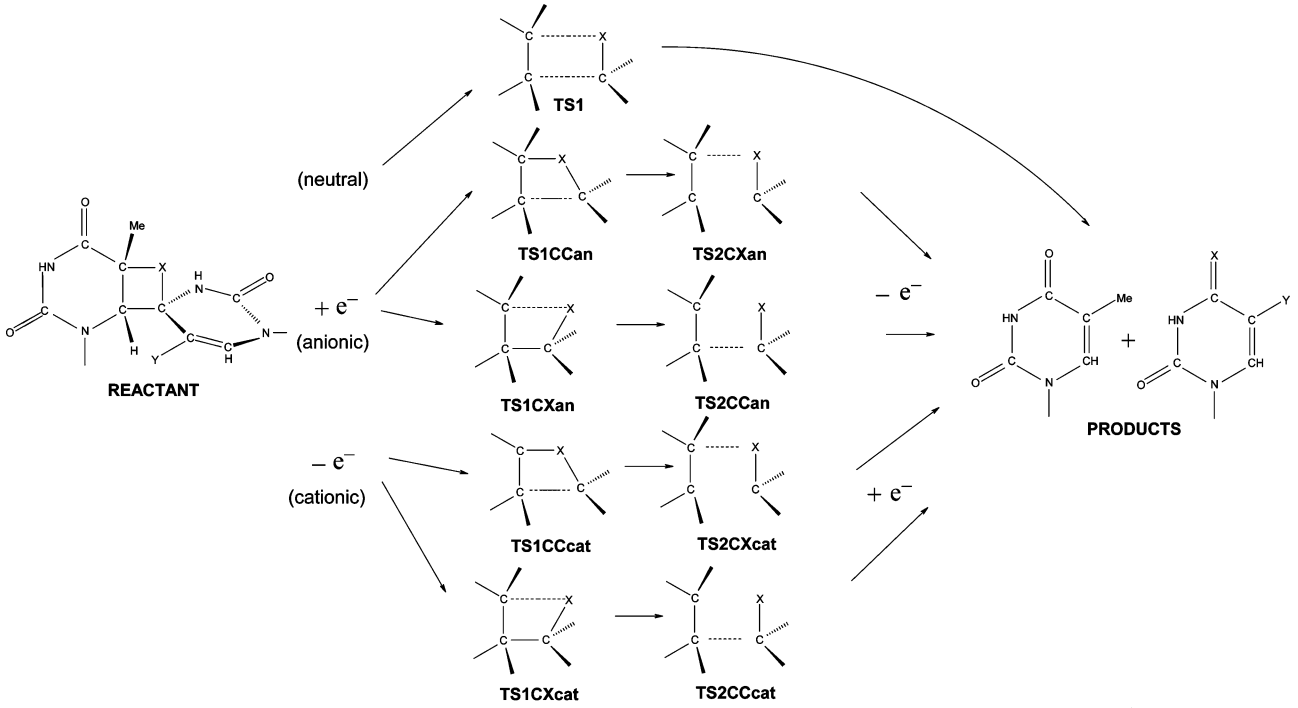

Figure 2. Anionic and cationic pathways for the fragmentation of cyclic oxetane and azetidine 6-4 lesions in UV-irradiated DNA by means of photoenzymic repair: X = O and Y = Me, fragmentation of T+T oxetane; X = NH and Y = H, fragmentation of T+C azetidine.

TABLE 1: Relative Electronic Energies (E_{elec}) of FAD in Different States, Electron Affinities and Ionization Potentials (EA and IP, at $T = 0$ K) of T+T Oxetane and T+C Azetidine and Energies of Reductive and Oxidative Electron Transfer (ΔE_{RED-ET} and ΔE_{OX-ET}) between $FADH^-(S_1)$ and T+T Oxetane and T+C Azetidine (All Values in kcal mol^{-1})

state	E_{elec}[a,b]	exp[c]	lesion	EA[a,d]	EA[d,e]	IP[a,f]	IP[e,f]	ΔE_{RED-ET}[g]	ΔE_{OX-ET}[g]
$FADH^-(S_0)$	0[h]	0	T+T oxetane (large model)	32.9	38.4	164.8	167.7	−56.6	203.5
$FADH^-(S_1)$	61.1[i]	57.3	T+C azetidine (large model)	0.4	5.8	140.6	144.8	−24.0	180.6
$FADH^{\bullet}$	42.9[h]		T+C azetidine (small model)	−7.4	1.7	147.6	151.5	−19.9	187.3
$FADH^{\bullet 2-}$	96.9[h]								

[a] B3LYP/6-311G(2df,p)//B3LYP/6-31G(d,p). [b] Calculations from ref 17. [c] Experimental data from ref 10. [d] The adiabatic electron affinity EA(M) of a species M is at $T = 0$ K given by $EA(M) = E_{elec}(M) + ZPVE(M) - E_{elec}(M^-) - ZPVE(M^-)$. [e] B3LYP/6-311+G(2df,p)//B3LYP/6-31G(d,p). [f] The adiabatic ionization potential IP(M) of a species M is at $T = 0$ K given by $IP(M) = E_{elec}(M^+) + ZPVE(M^+) - E_{elec}(M) - ZPVE(M)$. [g] Calculated using B3LYP/6-311+G(2df,p)//B3LYP/6-31G(d,p) data for EA and IP. [h] Adiabatic energy calculated using a geometry optimized for the state in question. [i] Vertical excitation energy calculated using a geometry optimized for $FADH^-(S_0)$ and a time-dependent DFT formalism.

Figure 2) and (ii) breakage of the C5−X4′ bond followed by breakage of the C6−C4 bond, below referred to as CX−CC and proceeding either via transition structures TS1CXan and TS2CCan (anionic pathway, Figure 2) or via TS1CXcat and TS2CCcat (cationic pathway, Figure 2). For closed-shell species, a concerted pathway involving the simultaneous fragmentation of the C6−C4′ and C5−X4′ bonds (proceeding via transition structure TS1) was investigated. This pathway corresponds to the thermal reversion of the concerted excited-state cycloaddition producing the 6-4 lesion[6] and represents an uncatalyzed fragmentation reaction. Accordingly, the resulting energetics were used as reference data relative to which the effect of ET was evaluated.

All calculations were carried out with the Gaussian 98[45] or Gaussian 03[46] suite of programs using the B3LYP hybrid density functional,[47−49] whose accuracy when applied to pericyclic reactions is well-documented.[50] Restricted and unrestricted formalisms were used for closed-shell and open-shell systems, respectively. Geometry optimization of stationary points (i.e., localization of minima and transition structures on the respective fragmentation potential energy surface (PES)) and frequency calculations to characterize the curvature of stationary points and to evaluate zero-point vibrational energy (ZPVE) and thermal enthalpy and free-energy corrections (at $T =$ 298.15 K) to the electronic energies were carried out with the 6-31G(d,p) double-ζ basis set. Single-point calculations were performed on the optimized geometries using the 6-311G(2df,p) and 6-311+G(2df,p) triple-ζ basis sets. Spin densities for open-shell systems were obtained from standard Mulliken population analysis using the latter of these basis sets, which includes diffuse s and p functions on second-row atoms and heavier.

In a set of preliminary calculations, the influence of the surrounding protein on the fragmentation reactions was modeled in an implicit fashion through B3LYP/6-311G(2df,p) single-point calculations employing different formulations of the polarizable continuum model (PCM),[51−53] with values ranging from 4 to 78 for the dielectric constant. The use of the PCM approach to represent bulk protein dielectric effects has provided results in nice agreement with experiments for a variety of enzymatic systems.[54] For the current substrates, the results turned out to be rather sensitive to the particular type of PCM calculation performed, which is likely related to the observation (see below) that the electron density distribution of the species under study changes significantly along the reaction coordinate. In order to keep the different systems as readily comparable as

possible and since our primary objective is to investigate intrinsic effects, we will herein focus on gas-phase data.

For a repair mechanism accomplished by reductive ET, it is worthwhile to also investigate whether protonation of the created radical anion affects its susceptibility toward cleavage. Consequently, the reactions of *neutral* T+C azetidine radicals were subjected to calculations as well. Given the size of the model system, the different fragmentation pathways, and the fact that three different atomic sites (the O2, O4, and O2′ carbonyl oxygens) are conceivable for protonation, it is clear that the investigation would be greatly facilitated by the use of a smaller computational model. Encouragingly, during the course of the project it was established that replacing the sugar-phosphate backbone by two hydrogen atoms results in a PES for the T+C azetidine radical anion that agrees qualitatively with that obtained by using the full model system (commented upon in detail below). Therefore, this smaller model was employed in the calculations investigating the effect of substrate protonation.

Results and Discussion

Electron-Transfer Reactions. Before presenting computed fragmentation PESs, it is informative to consider some data (Table 1) of relevance for the ET between the catalytic cofactor ($FADH^-$ in its lowest singlet excited state S_1) and the 6-4 lesions. From the point of view of either reductive or oxidative photoenzymic repair mechanisms, the ET reactions of interest are (similarly for T+C azetidine)

$$FADH^-(S_1) + \text{T+T oxetane} \xrightarrow{\text{reductive repair}} FADH^\bullet + \text{T+T oxetane radical anion} \quad (1)$$

$$FADH^-(S_1) + \text{T+T oxetane} \xrightarrow{\text{oxidative repair}} FADH^{\bullet 2-} + \text{T+T oxetane radical cation} \quad (2)$$

$FADH^\bullet$ is the deprotonated and oxidized radical form of $FADH_2$, and $FADH^{\bullet 2-}$ is the deprotonated and reduced radical form. Assuming that the excited $FADH^-$ is much more prone to donate an electron than to accept one, it may appear unlikely that an oxidative ET is realizable. However, it is interesting to note from studies of CPD photolyases that, even though an anionic reaction mechanism is commonly accepted for these enzymes, their complexes with CPD lesions have spectral properties compatible with the formation of $FADH^{\bullet 2-}$ during the repair process.[10]

From Table 1, we first note that the adiabatic B3LYP/6-311+G(2df,p)//B3LYP/6-31G(d,p) electron affinities (EA) of T+T oxetane (38.4 kcal mol^{-1}) and T+C azetidine (5.8 and 1.7 kcal mol^{-1} for the large and small computational model, respectively) are predicted to be *positive*. The observation that the anion radical is more stable than the parent closed-shell species has also been made for the T+T CPD system (EA $\approx$ 20 kcal mol^{-1})[17] and is a feature that facilitates reductive ET. DFT calculations on the DNA nucleobases indicate that there is a qualitative difference between the adiabatic EAs of T (positive by $\sim$3−4 kcal mol^{-1}) and C (negative by $\sim$0−2 kcal mol^{-1}),[55,56] which is likely reflected in the higher EA of T+T oxetane than of T+C azetidine. Without diffuse functions, the EAs obtained using the large models are lowered by about 5 kcal mol^{-1} (but are still positive), which is a consequence of a loss of stabilizing effect on the radicals. This effect is most pronounced for the small T+C azetidine model, resulting in an EA that is actually negative by 7.4 kcal mol^{-1}.

The adiabatic B3LYP/6-311+G(2df,p)//B3LYP/6-31G(d,p) ionization potentials (IP) of T+T oxetane and T+C azetidine, in turn, amount to 167.7 and 144.8 kcal mol^{-1} (151.5 kcal mol^{-1} for the small model), respectively. This is smaller than the 196 kcal mol^{-1} computed for the T+T CPD system[17] but nevertheless suggests that oxidative ET cannot proceed unless the S_1 state of $FADH^-$ has an appreciable electron affinity. The effect of diffuse functions is smaller on IPs than on EAs, as expected. It is worthwhile emphasizing that the small T+C azetidine model is qualitatively similar to the large one in terms of both EA and IP, provided that diffuse functions are employed.

Table 1 also includes relative electronic energies (E_{elec}) of the different states of the catalytic cofactor of relevance for reductive and oxidative ET, as obtained at the B3LYP/6-311G-(2df,p)//B3LYP/6-31G(d,p) level of theory.[17] The experimental absorption spectrum of enzyme-bound $FADH^-$ places the S_1 state at $\sim$57 kcal mol^{-1} above the ground state S_0.[10] Interestingly, the calculations on $FADH^-(S_1)$, which were carried out using time-dependent DFT (TD-DFT), yield an excitation energy (61.1 kcal mol^{-1}) that agrees with this result to within $\sim$4 kcal mol^{-1}. Since the theoretical estimate pertains to the absorption of $FADH^-$ in the gas phase, it is obvious that the excellent agreement between theory and experiment is partly fortuitous. Nevertheless, the accuracy of the calculation suggests that the ET energies of reactions (1) (ΔE_{RED-ET}) and (2) (ΔE_{OX-ET}) to a first approximation neglecting the influence of the surrounding protein and any electrostatic donor−acceptor interaction can be evaluated considering only intrinsic electron-donating/accepting properties as (using the data in Table 1)

$$\Delta E_{RED-ET} = -EA + E_{elec}[FADH^\bullet] - E_{elec}[FADH^-(S_1)] \quad (3)$$

$$\Delta E_{OX-ET} = IP + E_{elec}[FADH^{\bullet 2-}] - E_{elec}[FADH^-(S_1)] \quad (4)$$

Accordingly, one obtains ΔE_{RED-ET} values of −56.6 and −24.0 kcal mol^{-1} for T+T oxetane and T+C azetidine, respectively, which indicates that reductive ET is a favorable, downhill process. ET from a variety of electron-rich sensitizers to oxetane adducts of 1,3-dimethyluracil and different carbonyl compounds has been studied in fluorescence quenching experiments.[57] Through measurements of the decrease in fluorescence intensity of the sensitizer with increasing concentration of oxetane, quenching rate constants of the order of 10^9 M^{-1} s^{-1} (i.e., close to the diffusion limit) were obtained,[57] which suggests that reductive ET is also a very fast reaction.

The calculated values of ΔE_{OX-ET} (203.5 and 180.6 kcal mol^{-1}) indicate that oxidative ET, on the other hand, is a markedly unfavorable process. Therefore, it seems much more likely that the photoenzymic repair of 6-4 lesions is governed by an anionic reaction mechanism than a cationic. Even though the calculations may overestimate the values of ΔE_{OX-ET} or the effect of the protein environment may differ between reductive and oxidative ET, the accumulated error due to deficiencies in the gas-phase model system and quantum chemical methodology would have to be of the order of hundreds of kcal mol^{-1} for this conclusion to be incorrect. Also, the computational approach used herein has been shown to accurately reproduce experimental data for the thermodynamics of the anionic repair of T+T CPD lesions.[17]

In light of the prediction that $FADH^-$ cannot act as a hole donor in oxidative repair, it is worthwhile trying to estimate the potential of the *neutral* $FADH^\bullet$ form to fulfill this role, which one may expect to be better. Thus, using exactly the level of theory specified above, but noting that standard implementations of TD-DFT typically do not allow for excited states of radicals to be treated as rigorously and accurately as excited states of

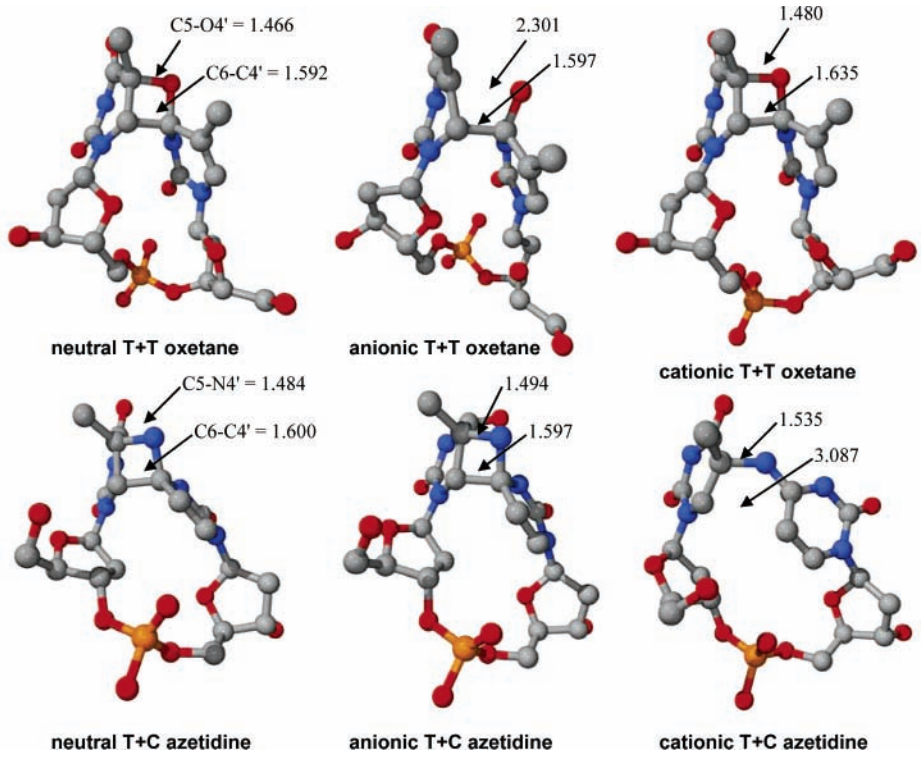

Figure 3. Optimized structures of different forms of T+T oxetane and T+C azetidine 6-4 lesions (hydrogen atoms are not displayed) corresponding to reactant complexes in Figure 4. Relevant bond lengths are given in Å.

closed-shell systems, we have also calculated the reaction energies for oxidative ET from T+T oxetane and T+C azetidine to the lowest excited-state of the $FADH^{\bullet}$ radical (producing $FADH^{-}$). The estimated -127.4 kcal mol^{-1} change in ΔE_{OX-ET} (ΔE_{OX-ET} [T+T oxetane] = 203.5 → 76.1, ΔE_{OX-ET} [T+C azetidine] = 180.6 → 53.2 kcal mol^{-1}) upon considering $FADH^{\bullet}$ instead of $FADH^{-}$ shows that the reactions would indeed be much less endothermic, albeit still not feasible, with $FADH^{\bullet}$ acting as the hole donor. As for reductive ET involving $FADH^{\bullet}$ (thus producing $FADH^{+}$) rather than $FADH^{-}$, in turn, the estimated 119.2 kcal mol^{-1} change in ΔE_{RED-ET} (ΔE_{RED-ET} [T+T oxetane] = -56.6 → 62.6, ΔE_{RED-ET} [T+C azetidine] = -24.0 → 95.2 kcal mol^{-1}) suggests that reductive repair requires that the catalytic cofactor carries a net negative charge. Loosely, this is consistent with the observation that the cofactor always assumes the $FADH^{-}$ form.[5−7,9,10]

Fragmentation Reactions: Potential Energy Surfaces. Having established that ET from the catalytic cofactor to the 6-4 lesion is favored over ET in the opposite direction on the basis of driving force, we now consider the susceptibility of the anionic and cationic radicals of T+T oxetane and T+C azetidine toward fragmentation along the pathways in Figure 2, in comparison with concerted fragmentation of the parent closed-shell species. The B3LYP/6-31G(d,p) structures of the different oxetane and azetidine forms are displayed in Figure 3 and correspond to reactant complexes (RC) in the different reactions. Figure 4 shows the computed PESs. Starting from the optimized RCs, transition structures (TS) were located by first performing a series of constrained B3LYP/6-31G(d,p) geometry optimizations (scans) along the reaction coordinates in question, with relevant bond lengths varied in steps of 0.1 Å. The resulting highest-energy structures were then used to start fully unconstrained TS optimizations. In addition to frequency calculations, the nature of the optimized TSs was also verified by means of intrinsic reaction coordinate calculations. In a number of cases, the scans either produced a set of structures with the electronic energy increasing monotonically, which indicates that the corresponding pathway is inaccessible, or yielded a highest-energy structure from which the TS optimization failed to locate a stationary point using default convergence criteria. For these cases, Figure 4 instead provides information obtained from the scans. In the remainder of this section, reported free energies are from B3LYP/6-311G(2df,p)//B3LYP/6-31G(d,p) and B3LYP/6-311+G(2df,p)//B3LYP/6-31G(d,p) calculations (the latter values will be given in parentheses).

From Figures 3 and 4, we observe that the C6−C4′ and C5−O4′ bond lengths of the closed-shell T+T oxetane are 1.59 and 1.47 Å, respectively. As indicated by experimental studies,[32] the calculations thus predict that the regeneration of the cyclic form of the T+T photoproduct in the initial event of 6-4 photolyase indeed produces a stable species. The intermonomeric C6−C4′ and C5−N4′ bonds in the closed-shell T+C azetidine are of similar lengths (1.60 and 1.48 Å, respectively). A concerted fragmentation of the oxetane (via TS1 at r_{CC} = 2.22; r_{CO} = 1.81 Å) has a significant free-energy barrier of 35.3 (35.0) kcal mol^{-1}, which basically prevents a thermally induced cycloreversion of this type of lesion. According to Woodward−Hoffmann theory,[58] the fragmentation could (in the absence of 6-4 photolyase) only proceed photochemically. However, such a reaction is less likely to take place, since the light-absorbing C5=C6 and C4′=O π-orbitals of the two reacting thymines have been transformed into σ-orbitals in the oxetane. Instead, 6-4 photolyases assist in the fragmentation by changing the charge of the lesion. While a fully optimized TS for the concerted fragmentation of the T+C azetidine could not be obtained, the initial scan (not shown in Figure 4) was indicative of an insurmountable energy barrier (>64 kcal mol^{-1}, E_{elec}) also for this reaction.

In the anionic T+T oxetane, the C5−O4′ bond is no longer intact (r_{CC} = 1.60; r_{CO} = 2.30 Å), which suggests that a photoenzymic repair mechanism mediated by reductive ET

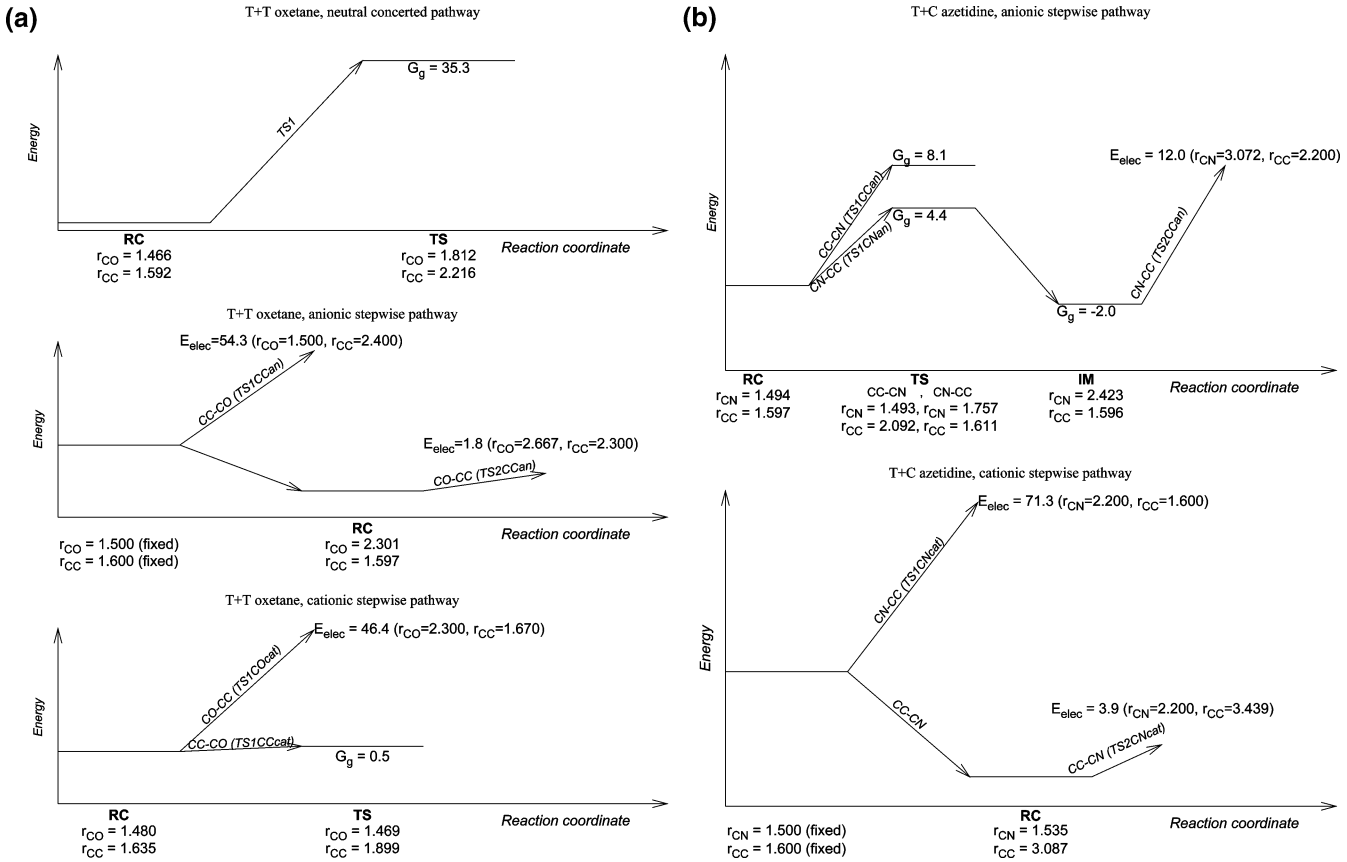

Figure 4. Schematic fragmentation PESs for (a) T+T oxetane and (b) T+C azetidine. Stationary points corresponding to reactant complexes (RC), transition structures (TS), or intermediates (IM) are indicated by horizontal lines. B3LYP/6-311G(2df,p)//B3LYP/6-31G(d,p) free energies (G_g, in kcal mol^{-1}) of TSs and IMs are given relative to the respective RC. Sloped arrows not leading to a stationary point represent a series of constrained B3LYP/6-31G(d,p) geometry optimizations with the electronic energy (E_{elec}, in kcal mol^{-1}) at the indicated geometry given relative to the structure at the origin of the arrow. Relevant bond lengths (r_{CC} = C6−C4′, r_{CO} = C5−O4′, and r_{CN} = C5−N4′) are given in Å.

would involve a barrierless cleavage of this bond as the first step. As for the the alternative CC−CO pathway involving splitting of the C6−C4′ bond via TS1CCan as the first step, a scan with the C5−O4′ bond held fixed at 1.5 Å and the C6−C4′ bond varied between 1.6 and 2.4 Å clearly showed that this pathway is inaccessible with the energy increasing monotonically throughout the series by more than 54 kcal mol^{-1} (E_{elec}) relative to the starting point. For the subsequent step of the preferred CO−CC pathway (splitting of the C6−C4′ bond via TS2CCan), a fully optimized TS could not be obtained. However, the highest-energy constrained structure (at r_{CC} = 2.30; r_{CO} = 2.67 Å) along this reaction coordinate has an energy which is only 2 kcal mol^{-1} (E_{elec}) higher than that of the RC. This indicates that the C6−C4′ bond fragmentation following the barrierless cleavage of the C5−O4′ bond is a very facile reaction and in fact suggests that reduction of the lesion readily restores (after ET back to FADH$^{\bullet}$) the parent thymines. A pronounced propensity for the four-membered ring of an anionic oxetane radical to fragment has also been demonstrated experimentally by Joseph and Falvey,[31] who measured a rate constant of $>2 \times 10^7$ s^{-1} (corresponding to a free-energy barrier of ∼7−8 kcal mol^{-1} at room temperature) for the cleavage of the adduct of 1,3-dimethyluracil and 1,N^4,N^4-trimethylcytosine.

Turning to the cationic T+T oxetane, we see from Figure 4 that oxidative ET lengthens (but does not cleave) the C6−C4′ bond, while the C5−O4′ bond remains largely unperturbed (r_{CC} = 1.59 → 1.64; r_{CO} = 1.47 → 1.48 Å). Accordingly, splitting of the C6−C4′ bond via TS1CCcat as the first step is expected to dominate over splitting of the C5−O4′ bond via TS1COcat. In fact, the estimated free-energy barrier (at r_{CC} = 1.90; r_{CO} = 1.47 Å) for C6−C4′ bond cleavage is only 0.5 (0.7) kcal mol^{-1}, whereas initial C5−O4′ bond cleavage is a prohibitively slow process (the energy is increasing monotonically by more than 46 kcal mol^{-1} (E_{elec}) during the initial scan). On the other hand, in regards to the C5−O4′ bond cleavage following the splitting of the C6−C4′ bond, constrained optimizations (not shown in Figure 4) showed that this reaction likely proceeds without a barrier. The propensity of cationic oxetanes to fragment via a CC−CO pathway has also been implicated in an experimental study of 2,3-diaryloxetanes.[36]

Apparently, the calculations on the different forms of T+T oxetane show that both reductive and oxidative ET facilitate the fragmentation of the four-membered ring considerably and that the order in which the bonds are broken depends on whether the lesion is reduced or oxidized. Reductive ET induces a CO−CC fragmentation pathway and oxidative ET a CC−CO pathway. Qualitatively, it is furthermore worthwhile emphasizing that the radical cation is predicted to fragment as readily as the radical anion. However, as we have already seen, an oxidative ET is not likely to take place.

While experimental data on fragmentation reactions of azetidine compounds are scarce, Carell and co-workers have, by comparing the reductive cleavage of a flavin-containing oxetane model compound with that of the corresponding thio-analogue thietane, reported that the reactions do not seem to depend on the type of heteroatom.[38] Thus, one may expect the anionic T+C azetidine to be similar to the anionic T+T oxetane regarding its tendency to fragment along a particular pathway. Indeed, the splitting of the intermonomeric bond involving the heteroatom as the first step appears to be a very facile reaction

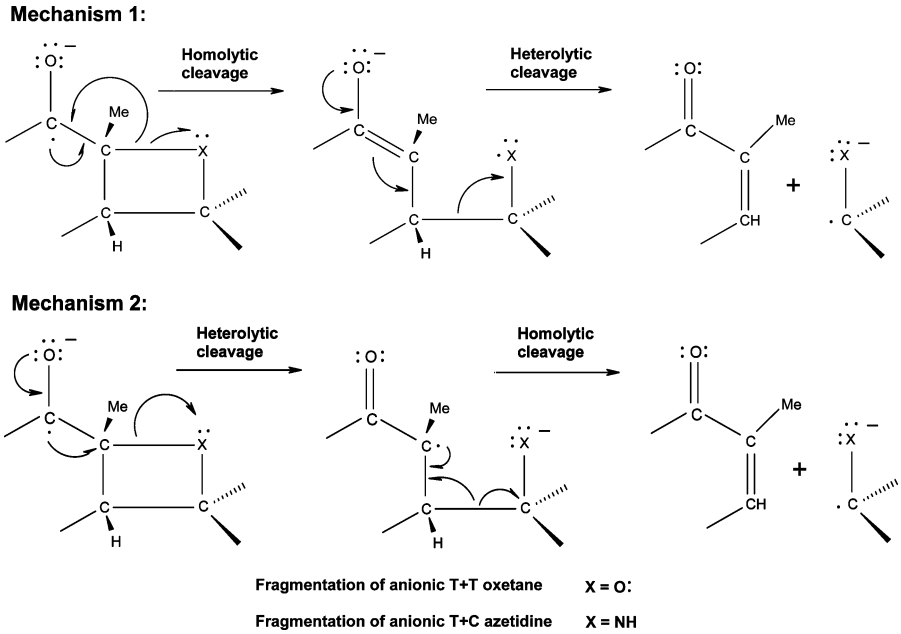

Figure 5. Reaction mechanisms for fragmentation of anionic T+T oxetane and T+C azetidine starting with C5−X4′ bond cleavage.

also in the azetidine system. However, in contrast to the barrierless cleavage of the C5−O4′ bond in the anionic oxetane, there is actually a transition structure TS1CNan (at $r_{CC} = 1.61$; $r_{CN} = 1.76$ Å) associated with a small free-energy barrier of 4.4 (2.0) kcal mol^{-1} for this process. Hence, whereas the oxetane C5−O4′ bond is cleaved spontaneously upon reduction, both intermonomeric bonds of the azetidine stay intact ($r_{CC} = 1.60$; $r_{CN} = 1.49$ Å). Furthermore, whereas the only available pathway for the anionic oxetane is CO−CC, fragmentation of the anionic azetidine initiated by C6−C4′ bond cleavage via TS1CCan (at $r_{CC} = 2.09$; $r_{CN} = 1.49$ Å) has a moderate 8.1 (6.6) kcal mol^{-1} free-energy barrier that, albeit higher than the 4.4 (2.0) kcal mol^{-1} required to surmount TS1CNan, does not exclude the possibility of a CC−CN fragmentation pathway in this system. The fact that the subsequent step of the CC−CN pathway (splitting of the C5−N4′ bond) through the initial scan (not shown in Figure 4) was found to occur without a barrier further underlines this point. Moreover, in analogy with the anionic oxetane system, the second step of the CN−CC pathway involving cleavage of the C6−C4′ does *not* occur without a barrier: surmounting the highest-energy constrained structure (at $r_{CC} = 2.20$; $r_{CN} = 3.07$ Å) along this reaction coordinate requires an activation energy of about 12 kcal mol^{-1} (E_{elec}) with respect to the IM (at $r_{CC} = 1.60$; $r_{CN} = 2.42$ Å). Although exceeding the 2 kcal mol^{-1} required by the oxetane, a barrier of this magnitude still corresponds to a reasonably fast reaction. In this context, it should be mentioned that a prediction of barrier size based on the electronic energy of a constrained structure is likely to overestimate the true barrier. Taken together, the data suggest that both CN−CC and CC−CN pathways enable facile fragmentation of the anionic T+C azetidine and that the cleavage of the C6−C4′ bond constitutes the kinetic bottleneck of both pathways.

Finally, considering the cationic T+C azetidine, we observe from Figures 3 and 4 that oxidative ET cleaves and lengthens the C6−C4′ and C5−N4′ bonds, respectively ($r_{CC} = 1.60 \rightarrow 3.09$; $r_{CN} = 1.48 \rightarrow 1.54$ Å). In analogy with the results for the cationic T+T oxetane, the calculations are indicative of this species readily undergoing fragmentation via a CC−CN pathway. The highest-energy constrained structure (at $r_{CC} = 3.44$; $r_{CN} = 2.20$ Å) along the C5−N4′ bond cleavage coordinate following C6−C4′ bond splitting lies only 4 kcal mol^{-1} (E_{elec}) above the RC.

Mechanistic Details of Reductive Fragmentation Reactions: Insight from Spin Density Analysis. The computed B3LYP/6-311+G(2df,p)//B3LYP/6-31G(d,p) spin densities discussed below shed light on the rearrangement in electron density distribution accompanying the fragmentation reactions of anionic T+T oxetane and T+C azetidine, and can be used to identify a particular C6−C4′ or C5−X4′ bond-breaking process as either homolytic or heterolytic. Without exception, the spin densities suggest that fragmentation of these bonds tends to localize the radical center to one of the atoms between which the bond was originally formed. If the bond is cleaved homolytically, one of its electrons will form the radical center of the fragmented species and the other an electron pair with the unpaired electron of the parent species. If the bond is cleaved heterolytically, the unpaired electron of the parent species redistributes to form the radical center of the fragmented species at the atomic site that otherwise would formally lose a unit negative charge by the other atom retaining both electrons of the bond.

As we have already seen, the only accessible fragmentation pathway for anionic T+T oxetane is CO−CC. Anionic T+C azetidine, on the other hand, may fragment either CN−CC or CC−CN. For the CX−CC bond fragmentation, two different reaction mechanisms are conceivable (Figure 5). In the first, homolytic C5−X4′ bond cleavage first creates a radical center at X4′ and a C4═C5 double bond. Heterolytic C6−C4′ bond cleavage then yields the canonical closed-shell form of one of the Pyrs by transforming the C5−C6 bond into a double bond, whereas the other Pyr is restored in an anionic open-shell form with the radical center at C4′. In the second mechanism, heterolytic C5−X4′ bond cleavage first creates a radical center at C5 and redistributes the negative charge from O4 to X4′. By the re-formation of the C5═C6 double bond and the shift of the radical center from C5 to C4′, homolytic C6−C4′ bond cleavage then yields the same species as the first mechanism.

For the anionic azetidine system, the RC of Figure 3 (with both intermonomeric bonds intact) has a spin density of 0.64 at C4, which is compatible with the schematic representation in Figure 5 of the electronic structure of the parent species. In the

TABLE 2: Comparison of Bond Lengths and Relative Electronic (E_{elec}), ZPVE-Corrected (E_0) and Free (G_g) Energies of Stationary Points on the Fragmentation PES for Anionic T+C Azetidine Radical Using Small and Large Model Systems (Bond Lengths in Å, Energies in kcal mol^{-1})

	RC		TS1CCan		TS1CNan	
model	small	large	small	large	small	large
C6−C4′	1.606	1.597	2.119	2.092	1.597	1.611
C5−N4′	1.576	1.494	1.488	1.493	1.740	1.757
$E_{elec}{}^a$	0.0	0.0	8.7	11.7	0.2	7.4
$E_{elec}{}^b$	0.0	0.0	10.0	10.2	1.0	5.0
$E_0{}^a$	0.0	0.0	7.6	9.0	−0.1	5.2
$E_0{}^b$	0.0	0.0	8.9	7.5	0.7	2.8
$G_g{}^a$	0.0	0.0	8.3	8.1	0.6	4.4
$G_g{}^b$	0.0	0.0	9.6	6.6	1.4	2.0

[a] B3LYP/6-311G(2df,p)//B3LYP/6-31G(d,p). [b] B3LYP/6-311+G(2df,p)//B3LYP/6-31G(d,p).

IM following C5−N4′ bond cleavage, the N4′ spin density amounts to 0.56 (0.00 in the RC) and the C4−C5 bond length equals 1.41 Å (1.54 Å). These results suggest that the CN−CC pathway proceeds by way of the first (i.e., homolytic−heterolytic) mechanism.

For the anionic oxetane system, in turn, the RC of Figure 3 has a spin density at C4 of only 0.05. This is because the C5−O4′ bond is broken and the unpaired electron instead resides at C5 (with spin density 0.54). Nevertheless, the transient species that precedes the fragmentation of the C5−O4′ bond should be very similar electronically to that of the corresponding azetidine and hence should also be compatible with either of the reaction mechanisms outlined in Figure 5. The C5 spin density (0.54) and O4′ charge (−0.55) suggest that the CO−CC pathway proceeds by way of the second (i.e., heterolytic−homolytic) mechanism. Thus, depending on the heteroatom, CX−CC fragmentation of the anionic lesions appears to be governed by different mechanisms. In this regard, the higher electronegativity of oxygen is likely an important factor and may enable the oxetane C5−O4′ bond to undergo heterolytic rather than homolytic cleavage. Furthermore, considering that the second step of the azetidine CN−CC pathway involving heterolytic fragmentation of the C6−C4′ bond (cf. Figure 5) is associated with a non-negligible energy barrier of about 12 kcal mol^{-1} (E_{elec}), it seems reasonable to attribute the observation that anionic T+C azetidine thereby does not fragment as readily as anionic T+T oxetane to the difference in electronegativity between nitrogen and oxygen.

Fragmentation of T+C Azetidine Radical Anion: Evaluation of the Small Model System. As noted in a previous section, the IP and EA calculated using the small T+C azetidine model are in qualitative agreement (to within ∼7 and ∼4 kcal mol^{-1}, respectively) with the IP and EA obtained using the large model, provided that diffuse functions are included in the single-point energy evaluation. In order to further ascertain whether it is possible to facilitate the investigation of the effect of substrate protonation on the reductive fragmentation of T+C azetidine by replacing the sugar-phosphate backbone by two hydrogen atoms, Table 2 compares key features of the fragmentation PES as obtained by employing the small and large model of the anion, respectively.

Assessing the first step of the CC−CN and CN−CC pathways, we first observe that the optimized C6−C4′ and C5−N4′ bond lengths of the RC, TS1CCan, and TS1CNan are relatively insensitive to the size of the model system. With the exception of the RC C5−N4′ bond, which is as much as 0.08 Å longer in the small model, no bond length varies more than 0.03 Å with system size. Furthermore, the energy barriers for C6−C4′ and C5−N4′ bond cleavage are not significantly altered by the use of a smaller model. For TS1CCan, the difference in barrier height is at most 3.0 kcal mol^{-1}, regardless of whether electronic, ZPVE-corrected, or free energies are considered. For TS1CNan, the long RC C5−N4′ bond of the small model is reflected in a lowering of the electronic barrier by 7.2 kcal mol^{-1} at the 6-311G(2df,p) basis-set level. However, with the use of diffuse functions and inclusion of ZPVE and thermal corrections, the magnitude of this geometric effect is reduced considerably. Moreover, in line with the results for the large model, we observe that the calculations predict that C5−N4′ bond cleavage is kinetically favored over C6−C4′ bond cleavage.

As for the second step of the CC−CN and CN−CC pathways, the small model system was of limited use. Because of its higher conformational flexibility, it was actually not possible to reliably perform any of the geometry optimizations required to investigate C5−N4′ and C6−C4′ bond cleavage via TS2CNan and TS2CCan. However, this deficiency does not invalidate the use of a small model for investigating the effect of substrate protonation since (a) the corresponding models of the protonated species were perfectly amenable to exploration of the *full* fragmentation reaction and (b) the qualitative conclusions thereby drawn are based on results for the *first* step of the two pathways.

Proton-Transfer Reactions of T+C Azetidine Radicals. Before the discussion of the results directly pertaining to the influence of protonation on reductive fragmentation, the calculated adiabatic proton affinities (PA) given in Table 3 provide some information as to the most likely atomic site (the O2, O4, or O2′ carbonyl oxygen) for protonation of the T+C azetidine radical anion at the RC geometry. Accordingly, O4 is the preferred site by ∼6−8 and ∼11−12 kcal mol^{-1} over O2 and O2′, respectively. Using diffuse functions, the PAs are lowered by ∼8−9 kcal mol^{-1}, which implies that the anionic radicals thereby gain more stabilization than the neutral radicals. This suggests that the unpaired electron is stabilized by an added proton.

In order to assess whether *deprotonation* of the radical cation created by an oxidative ET is likely to take place, we have also calculated PAs of neutral T+C azetidine radicals. Since an oxidative ET primarily reduces the electron density between C5′ and C6′, the moieties of interest in this regard are C5′H or C6′H. The computed PAs corresponding to the regeneration of the parent species indicate that deprotonation of the azetidine radical cation is not, as opposed to protonation of the azetidine radical anion, a favorable process. Of course, albeit informative, this is a limited analysis in that it refers only to protonation and deprotonation as governed by the intrinsic properties of the radicals and does not take into account that the amino acid composition of the surrounding enzyme in the vicinity of the lesion may well favor one process over the other. Unfortunately, no enzyme−substrate complex has yet been structurally resolved by X-ray crystallography to identify thereby relevant interactions.[59]

Effect of Protonation on Reductive Fragmentation of T+C Azetidine. With the use of the small computational model, Table 4 summarizes the calculations on the neutral T+C azetidine radicals, in comparison with those on the anionic radical. Considering first protonation at the preferred O4 site, we observe that this significantly increases the free-energy barriers associated with cleavage of the C6−C4′ and C5−N4′

TABLE 3: Proton Affinities (PA, in kcal mol^{-1}) of Anionic and Neutral T+C Azetidine Radicals at T = 298.15 K Using the Small Model System

	site of protonation	PA[a,c,d]	PA[b,c,d]
RC Geometry			
anionic T+C azetidine radical + H^+ → neutral T+C azetidine radical-protO2	O2	330.0	320.7
anionic T+C azetidine radical + H^+ → neutral T+C azetidine radical-protO4	O4	336.4	328.4
anionic T+C azetidine radical + H^+ → neutral T+C azetidine radical-protO2′	O2′	325.7	316.8
neutral T+C azetidine radical-deprotC6′ + H^+ → cationic T+C azetidine radical	C6′	277.5	277.9
neutral T+C azetidine radical-deprotC5′ + H^+ → cationic T+C azetidine radical	C5′	280.6	273.7
TS1 Geometry			
TS1CCan: anionic T+C azetidine radical + H^+ → neutral T+C azetidine radical-protO2	O2	319.4 (−10.6)	311.4 (−9.3)
TS1CCan: anionic T+C azetidine radical + H^+ → neutral T+C azetidine radical-protO4	O4	314.6 (−21.8)	308.2 (−20.2)
TS1CCan: anionic T+C azetidine radical + H^+ → neutral T+C azetidine radical-protO2′	O2′	309.6 (−16.1)	301.1 (−15.7)
TS1CNan: anionic T+C azetidine radical + H^+ → neutral T+C azetidine radical-protO2	O2	304.7 (−25.3)	298.0 (−22.7)
TS1CNan: anionic T+C azetidine radical + H^+ → neutral T+C azetidine radical-protO4	O4	324.9 (−11.5)	317.5 (−10.9)
TS1CNan: anionic T+C azetidine radical + H^+ → neutral T+C azetidine radical-protO2′	O2′	295.5 (−30.2)	289.8 (−27.0)

[a] B3LYP/6-311G(2df,p)//B3LYP/6-31G(d,p). [b] B3LYP/6-311+G(2df,p)//B3LYP/6-31G(d,p). [c] The adiabatic proton affinity PA(M) of a species M is at a finite temperature T given in terms of enthalpies as PA(M) = $-[H(MH^+) - H(M) - 5RT/2]$, where R is the molar gas constant. [d] PA(TS1) − PA(RC) in parentheses.

TABLE 4: Comparison of Bond Lengths and Relative Electronic (E_{elec}), ZPVE-Corrected (E_0) and Free (G_g) Energies for Stationary Points on the Fragmentation PESs for Anionic and Neutral T+C Azetidine Radicals Using the Small Model System (Bond Lengths in Å, Energies in kcal mol^{-1})

		CC−CN pathway			CN−CC pathway		
	RC	TS1CCan	IM	TS2CNan	TS1CNan	IM	TS2CCan
Anionic T+C Azetidine Radical							
C6−C4′	1.606	2.119			1.597		
C5−N4′	1.576	1.488			1.740		
E_{elec}[a]	0.0	9.6, 8.7, 10.0	convergence problems		0.4, 0.2, 1.0	convergence problems	
E_0[b], G_g[b]	0.0	7.6, 8.3			−0.1, 0.6		
Neutral T+C Azetidine Radical-ProtO2							
C6−C4′	1.606	2.299	2.961	3.032	1.587		
C5−N4′	1.496	1.491	1.556	1.759	2.042		
E_{elec}[a]	0.0	21.5, 19.8, 19.8	14.0, 10.8, 10.9	14.6, 10.9, 10.9	29.9, 26.6, 24.8	convergence problems	
E_0[b], G_g[b]	0.0	18.0, 17.9	8.8, 7.5	8.1, 7.2	24.2, 22.8		
Neutral T+C Azetidine Radical-ProtO4							
C6−C4′	1.595	2.414			1.582	1.586	1.912
C5−N4′	1.492	1.492			2.019	3.067	3.106
E_{elec}[a]	0.0	33.3, 31.5, 31.3	not investigated		13.4, 12.3, 12.5	−1.6, −2.8, −2.6	2.5, 0.6, 0.6
E_0[b], G_g[b]	0.0	29.1, 29.3			11.6, 11.5	−3.4, −3.5	−1.1, −1.0
Neutral T+C Azetidine Radical-ProtO2'							
C6−C4′	1.601	2.339	2.900	2.985	1.574		
C5−N4′	1.488	1.480	1.531	1.661	1.969		
E_{elec}[a]	0.0	26.5, 25.4, 26.5	21.3, 19.7, 21.1	22.0, 20.1, 21.3	33.7, 32.0, 29.6	barrierless second step	
E_0[b], G_g[b]	0.0	23.9, 24.6	18.5, 18.5	18.0, 18.2	29.3, 28.6		

[a] B3LYP single-point calculations using the 6-31G(d,p), 6-311G(2df,p), and 6-311+G(2df,p) basis sets, respectively. [b] B3LYP/6-311G(2df,p)//B3LYP/6-31G(d,p).

bonds (TS1CCan, 8.3 → 29.3; TS1CNan, 0.6 → 11.5 kcal mol^{-1}) and in fact renders the CC−CN pathway inaccessible. This is in contrast to the anionic system, for which both CN−CC and CC−CN pathways appear to enable facile fragmentation. The second step (via TS2CCan) of the CN−CC pathway maintains a low free-energy barrier of 2.5 kcal mol^{-1} relative to the IM even after protonation.

Since the difference in enthalpy of activation between the reactions of the O4-protonated and anionic radical equals the difference in adiabatic PA (at O4) between the anionic RC and TS in question, i.e.,

$$\Delta\Delta H^{\ddagger} = \Delta H^{\ddagger}_{O4-prot} - \Delta H^{\ddagger}_{an} = H_{TS-O4-prot} - H_{RC-O4-prot} - H_{TS-an} + H_{RC-an} = PA_{RC-an} - PA_{TS-an} \quad (5)$$

the increase in fragmentation free-energy barriers for the O4-protonated radical can (neglecting entropy effects) be attributed to the RC being more stabilized by protonation than TS1CCan and TS1CNan. In addition to PAs of the anionic T+C azetidine radical at the RC geometry, Table 3 also lists the corresponding PAs at the optimized TS1CCan and TS1CNan geometries. We observe that the RC PAs throughout are higher (by ∼9−27 or ∼11−30 kcal mol^{-1}, depending on the basis set) than the TS1CCan and TS1CNan PAs. Accordingly, as detailed in Table 4, also protonation at O2/O2′ increases the free-energy barriers (TS1CCan, 8.3 → 17.9/24.6; TS1CNan, 0.6 → 22.8/28.6 kcal mol^{-1}). Hence, although less favorable than O4-protonation, these processes are also predicted to slow down the fragmentation reactions considerably and actually appear to change the preferred mechanism from CN−CC to CC−CN. For both the O2 and O2′-protonated radical the second step (via TS2CNan) of the CC−CN pathway has a very small energy barrier of less than 1 kcal mol^{-1} (E_{elec}) relative to the respective IM that vanishes when ZPVE and thermal corrections are accounted for.

Protonation has a pronounced effect on the spin density distribution in the azetidine radicals and localizes the unpaired electron to the carbon atom of the protonated carbonyl group.

Thus, while C4 of the anionic radical at the RC geometry has a spin density of 0.55, C2 of the O2-protonated, C4 of the O4-protonated, and C2′ of the O2′-protonated radical have spin densities of 0.73, 0.86, and 0.76, respectively. Given that the added proton exerts a stabilizing effect on the unpaired electron, as indicated by calculations using diffuse functions resulting in lowered PAs, the fact that TS1CCan and TS1CNan are less stabilized by protonation than RC can partly be rationalized in terms of the fragmentation reactions inevitably requiring electronic rearrangement involving allocation of the unpaired electron to other atomic sites than C2, C4, and C2′.

Conclusions

We have in the present work explored anionic and cationic reaction mechanisms for the photoenzymic repair of 6-4 photoproducts in UV-damaged DNA by means of density functional calculations. By investigation of the repair of one oxetane (T+T) and one azetidine (T+C) lesion, it is found that the ET processes underlying the two mechanisms have markedly different reaction energies: while reductive ET from the catalytic cofactor of the enzyme ($FADH^-$) to the lesions initiating an anionic mechanism is a favorable process with an appreciable driving force, oxidative ET in the opposite direction initiating a cationic mechanism is likely made impossible by the resulting species ($FADH^{\bullet 2-}$ and T+T oxetane/T+C azetidine radical cation) lying significantly higher in energy than the corresponding species produced by the reductive ET ($FADH^{\bullet}$ and T+T oxetane/T+C azetidine radical anion).

Furthermore, it is shown that the formation of open-shell forms of the 6-4 lesions via reduction *as well as* oxidation has a considerable catalyzing effect on the fragmentation into monomeric Pyrs, with energy barriers being either reduced to a few kcal mol^{-1} (anionic and cationic T+T oxetane, cationic T+C azetidine) or lowered into the ∼10 kcal mol^{-1} regime (anionic T+C azetidine). Moreover, the sequence of intermonomeric bond cleavages depends on whether the lesion is reduced or oxidized. Anionic T+T oxetane can only fragment along a pathway (CO−CC) involving first C5−O4′ and then C6−C4′ bond cleavage, whereas fragmentation of the cation proceeds CC−CO. Anionic T+C azetidine, in turn, can fragment both CN−CC (first C5−N4′ and then C6−C4′) and CC−CN, but the cation only CC−CN. For the anionic radicals, the calculations are indicative of the bonds being cleaved by different mechanisms along the oxetane CO−CC (heterolytic followed by homolytic) and azetidine CN−CC (homolytic followed by heterolytic) pathways.

Finally, from calculations on the resulting neutral radicals, it is inferred that protonation of the T+C azetidine radical anion at O2, O4, or O2′ significantly increases the free-energy barriers associated with (but does not prevent) fragmentation of the C5−N4′ and C6−C4′ bonds and that this effect can be attributed to anionic RCs being more stabilized by protonation than anionic TSs.

Acknowledgment. We thank the supercomputer facilities in Linköping (NSC) and Stockholm (PDC) for grants of computer time. L.A.E. and B.D. acknowledge financial support from the Swedish Research Council (VR).

References and Notes

(1) Taylor, J.-S. *Acc. Chem. Res.* **1994**, *27*, 76−82.
(2) Reardon, J. T.; Sancar, A. *Genes Dev.* **2003**, *17*, 2539−2551.
(3) Kamiya, H.; Iwai, S.; Kasai, H. *Nucleic Acids Res.* **1998**, *26*, 2611−2617.
(4) Lysetska, M.; Knoll, A.; Boehringer, D.; Hey, T.; Krauss, G. *Nucleic Acids Res.* **2002**, *30*, 2686−2691.
(5) Sancar, A. *Chem. Rev.* **2003**, *103*, 2203−2237.
(6) Carell, T.; Burgdorf, L. T.; Kundu, L. M.; Cichon, M. *Curr. Opin. Chem. Biol.* **2001**, *5*, 491−498.
(7) Begley, T. P. *Acc. Chem. Res.* **1994**, *27*, 394−401.
(8) Sancar, A.; Sancar, G. B. *Annu. Rev. Biochem.* **1988**, *57*, 29−67.
(9) Sancar, A. *Biochemistry* **1994**, *33*, 2−9.
(10) Heelis, P. F.; Hartman, R. F.; Rose, S. D. *Chem. Soc. Rev.* **1995**, *24*, 289−297.
(11) Miaskiewicz, K.; Miller, J.; Cooney, M.; Osman, R. *J. Am. Chem. Soc.* **1996**, *118*, 9156−9163.
(12) Sanders, D. B.; Wiest, O. *J. Am. Chem. Soc.* **1999**, *121*, 5127−5134.
(13) Harrison, C. B.; O'Neil, L. L.; Wiest, O. *J. Phys. Chem. A* **2005**, *109*, 7001−7012.
(14) Voityuk, A. A.; Michel-Beyerle, M. E.; Rösch, N. *J. Am. Chem. Soc.* **1996**, *118*, 9750−9758.
(15) Rak, J.; Voityuk, A. A.; Michel-Beyerle, M. E.; Rösch, N. *J. Phys. Chem. A* **1999**, *103*, 3569−3574.
(16) Aida, M.; Inoue, F.; Kaneko, M.; Dupuis, M. *J. Am. Chem. Soc.* **1997**, *119*, 12274−12279.
(17) Durbeej, B.; Eriksson, L. A. *J. Am. Chem. Soc.* **2000**, *122*, 10126−10132.
(18) Durbeej, B.; Eriksson, L. A. *J. Photochem. Photobiol., A* **2002**, *152*, 95−101.
(19) Durbeej, B.; Eriksson, L. A. *Photochem. Photobiol.* **2003**, *78*, 159−167.
(20) Hartman, R. F.; Rose, S. D. *J. Am. Chem. Soc.* **1992**, *114*, 3559−3560.
(21) Dandliker, P. J.; Holmlin, R. E.; Barton, J. K. *Science* **1997**, *275*, 1465−1468.
(22) Gilbert, A.; Baggot J. *Essentials of Molecular Photochemistry*; Blackwell Scientific Publications: Oxford, U.K., 1991.
(23) Heelis, P. F.; Liu, S. *J. Am. Chem. Soc.* **1997**, *119*, 2936−2937.
(24) Kimura, S.; Tahira, Y.; Ishibashi, T.; Mori, Y.; Mori, T.; Hashimoto, J.; Sakaguchi, K. *Nucleic Acids Res.* **2004**, *32*, 2760−2767.
(25) Todo, T.; Takemori, H.; Ryo, H.; Ihara, M.; Matsunaga, T.; Nikaido, O.; Sato, K.; Nomura, T. *Nature* **1993**, *361*, 371−374.
(26) Zhao, X.; Liu, J.; Hsu, D. S.; Zhao, S.; Taylor, J.-S.; Sancar, A. *J. Biol. Chem.* **1997**, *272*, 32580−32590.
(27) Kim, S. T.; Malhotra, K.; Smith, C. A.; Taylor, J.-S.; Sancar, A. *J. Biol. Chem.* **1994**, *269*, 8535−8580.
(28) Hitomi, K.; Kim, S. T.; Iwai, S.; Harima, N.; Otoshi, E.; Ikenaga, M.; Todo, T. *J. Biol. Chem.* **1997**, *272*, 32591−32598.
(29) Nakajima, S.; Sugiyama, M.; Iwai, S.; Hitomi, K.; Otoshi, E.; Kim, S. T.; Jiang, C. Z.; Todo, T.; Britt, A. B.; Yamamoto, K. *Nucleic Acids Res.* **1998**, *26*, 638−644.
(30) Cichon, M. K.; Arnold, S.; Carell, T. *Angew. Chem., Int. Ed.* **2002**, *41*, 767−770.
(31) Joseph, A.; Falvey, D. E. *Photochem. Photobiol. Sci.* **2002**, *1*, 632−635.
(32) Clivio, P.; Fourrey, J. L. *Chem. Commun*. **1996**, 2203−2204.
(33) Todo, T.; Ryo, H.; Yamamoto, K.; Toh, H.; Inui, T.; Ayaki, H.; Nomura, T.; Ikenaga, M. *Science* **1996**, *272*, 109−112.
(34) Vande Berg, B. J.; Sancar, G. B. *J. Biol. Chem.* **1998**, *273*, 20276−20284.
(35) Hitomi, K.; Nakamura, H.; Kim, S. T.; Mizukoshi, T.; Ishikawa, T.; Iwai, S.; Todo, T. *J. Biol. Chem.* **2001**, *276*, 10103−10109.
(36) Izquierdo, M. A.; Miranda, M. A. *Eur. J. Org. Chem*. **2004**, 1424−1431.
(37) Pérez-Ruiz, R.; Izquierdo, M. A.; Miranda, M. A. *J. Org. Chem.* **2003**, 10103−10108.
(38) Friedel, M. G.; Cichon, M. K.; Carell, T. *Org. Biomol. Chem.* **2005**, *3*, 1937−1941.
(39) Stafforst, T.; Diederichsen, U. *Chem. Commun.* **2005**, 3430−3432.
(40) Wang, Y.; Gaspar, P. P.; Taylor, J.-S. *J. Am. Chem. Soc.* **2000**, *122*, 5510−5519.
(41) Izquierdo, M. A.; Domingo, L. R.; Miranda, M. A. *J. Phys. Chem. A* **2005**, *109*, 2602−2607.
(42) Joseph, A.; Prakash, G.; Falvey, D. E. *J. Am. Chem. Soc.* **2000**, *122*, 11219−11225.
(43) Miranda, M. A.; Izquierdo, M. A. *J. Am. Chem. Soc.* **2002**, *124*, 6532−6533.
(44) Miranda, M. A.; Izquierdo, M. A.; Galindo, F. *J. Org. Chem.* **2002**, *67*, 4138−4142.
(45) Frisch, M. J.; Trucks, G. W.; Schlegel, H. B.; Scuseria, G. E.; Robb, M. A.; Cheeseman, J. R.; Zakrzewski, V. G.; Montgomery, J. A., Jr.; Stratmann, R. E.; Burant, J. C.; Dapprich, S.; Millam, J. M.; Daniels, A. D.; Kudin, K. N.; Strain, M. C.; Farkas, O.; Tomasi, J.; Barone, V.; Cossi, M.; Cammi, R.; Mennucci, B.; Pomelli, C.; Adamo, C.; Clifford, S.; Ochterski, J.; Petersson, G. A.; Ayala, P. Y.; Cui, Q.; Morokuma, K.; Malick, D. K.; Rabuck, A. D.; Raghavachari, K.; Foresman, J. B.; Cioslowski, J.;

Ortiz, J. V.; Stefanov, B. B.; Liu, G.; Liashenko, A.; Piskorz, P.; Komaromi, I.; Gomperts, R.; Martin, R. L.; Fox, D. J.; Keith, T.; Al-Laham, M. A.; Peng, C. Y.; Nanayakkara, A.; Gonzalez, C.; Challacombe, M.; Gill, P. M. W.; Johnson, B. G.; Chen, W.; Wong, M. W.; Andres, J. L.; Head-Gordon, M.; Replogle, E. S.; Pople, J. A. *Gaussian 98*, revision A.11.4; Gaussian, Inc.: Pittsburgh, PA, 2002.

(46) Frisch, M. J.; Trucks, G. W.; Schlegel, H. B.; Scuseria, G. E.; Robb, M. A.; Cheeseman, J. R.; Montgomery, J. A., Jr.; Vreven, T.; Kudin, K. N.; Burant, J. C.; Millam, J. M.; Iyengar, S. S.; Tomasi, J.; Barone, V.; Mennucci, B.; Cossi, M.; Scalmani, G.; Rega, N.; Petersson, G. A.; Nakatsuji, H.; Hada, M.; Ehara, M.; Toyota, K.; Fukuda, R.; Hasegawa, J.; Ishida, M.; Nakajima, T.; Honda, Y.; Kitao, O.; Nakai, H.; Klene, M.; Li, X.; Knox, J. E.; Hratchian, H. P.; Cross, J. B.; Bakken, V.; Adamo, C.; Jaramillo, J.; Gomperts, R.; Stratmann, R. E.; Yazyev, O.; Austin, A. J.; Cammi, R.; Pomelli, C.; Ochterski, J. W.; Ayala, P. Y.; Morokuma, K.; Voth, G. A.; Salvador, P.; Dannenberg, J. J.; Zakrzewski, V. G.; Dapprich, S.; Daniels, A. D.; Strain, M. C.; Farkas, O.; Malick, D. K.; Rabuck, A. D.; Raghavachari, K.; Foresman, J. B.; Ortiz, J. V.; Cui, Q.; Baboul, A. G.; Clifford, S.; Cioslowski, J.; Stefanov, B. B.; Liu, G.; Liashenko, A.; Piskorz, P.; Komaromi, I.; Martin, R. L.; Fox, D. J.; Keith, T.; Al-Laham, M. A.; Peng, C. Y.; Nanayakkara, A.; Challacombe, M.; Gill, P. M. W.; Johnson, B.; Chen, W.; Wong, M. W.; Gonzalez, C.; Pople, J. A. *Gaussian 03*, revision B.05; Gaussian, Inc.: Wallingford, CT, 2004.

(47) Lee, C.; Yang, W.; Parr, R. G. *Phys. Rev. B* **1988**, *37*, 785−789.

(48) Becke, A. D. *J. Chem. Phys.* **1993**, *98*, 5648−5652.

(49) Stevens, P. J.; Devlin, F. J.; Chabalowski, C. F.; Frisch, M. J. *J. Phys. Chem.* **1994**, *98*, 11623−11627.

(50) Wiest, O.; Montiel, D. C.; Houk, K. N. *J. Phys. Chem. A* **1997**, *101*, 8378−8388.

(51) Tomasi, J.; Persico, M. *Chem. Rev.* **1994**, *94*, 2027−2094.

(52) Cramer, C. J.; Truhlar, D. G. *Chem. Rev.* **1999**, *99*, 2161−2200.

(53) Tomasi, J.; Mennucci, B.; Cammi, R. *Chem. Rev.* **2005**, *105*, 2999−3093.

(54) Siegbahn, P. E. M.; Blomberg, M. R. A. *Chem. Rev.* **2000**, *100*, 421−437.

(55) Wetmore, S. D.; Boyd, R. J.; Eriksson, L. A. *Chem. Phys. Lett.* **2000**, *322*, 129−135.

(56) Wesolowski, S. S.; Leininger, M. L.; Pentchev, P. N.; Schaefer, H. F., III, *J. Am. Chem. Soc.* **2001**, *123*, 4023−4028.

(57) Song, Q.; Hei, X.; Xu, Z.; Zhang, X.; Guo, Q. *Bioorg. Chem.* **2003**, *31*, 357−366.

(58) Woodward, R. B.; Hoffman, R. *The Conservation of Orbital Symmetry*; Verlag Chemie: Berlin, 1970.

(59) Weber, S. *Biochim. Biophys. Acta* **2005**, *1707*, 1−23.